Chapter 6

WST-1 Reduction at the RBC Plasma Membrane

6.1 Background

Tetrazolium dyes have often been used as electron acceptors in measurements of cell proliferation rates (Berridge and Tan, 1993; Ishiyama, *et al.*, 1993; Berridge, *et al.*, 1996), in histochemical procedures (Zamudio, *et al.*, 1969; May, *et al.*, 1995b; Demehin, *et al.*, 2001), and for assaying redox enzymes (Berridge and Tan, 1993; Mittler and Zilinskas, 1993; Debnam and Shearer, 1997; Ye, *et al.*, 1997; Berridge and Tan, 1998, 2000a, 2000b; Ukeda, *et al.*, 1999; Peskin and Winterbourn, 2000; Tan and Berridge, 2000; Demehin, *et al.*, 2001; Baker, *et al.*, 2004a). On reduction, tetrazolium salts produce a highly coloured end-product called formazan. In general, tetrazolium salts are soluble due to the cationic character of their heterocyclic ring, whereas the formazan products are electrically neutral and insoluble in water (Ishiyama, *et al.*, 1993). The development of tetrazolium salts that are reduced to water soluble formazans (Ishiyama, *et al.*, 1993) has broadened the appeal of these redox dyes.

The water soluble tetrazolium 4-[3-(4-iodophenyl)-2-(4-nitrophenyl)-2*H*-5-tetrazolio]-1,3-benzene disulfonate (WST-1; Figure 6.1) developed by Ishiyama and co-workers (1993), on reduction, produces a formazan that is water soluble due to the two negatively charged sulfonate groups. At pH 8.0 the formazan has an absorbance maximum (λ_{max}) at 438 nm and a molar extinction coefficient of 37 $mM^{-1}cm^{-1}$. At higher pH the λ_{max} shifts from 438 nm to 593 nm due to deprotonation of the secondary amine (Ishiyama, *et al.*, 1993). WST-1 is reduced in the presence of 1-methoxy PMS (or PMS) and NADH. This reduction is optimal at pH 8.5–10.5 and does not reach completion at more acidic pH (Ishiyama, *et al.*, 1993). WST-1 can

also be chemically reduced by dithiothrietol, mercaptoethanol, L-cysteine and L-ascorbic acid and to a lesser extent by GSH (Berridge, *et al.*, 1996).

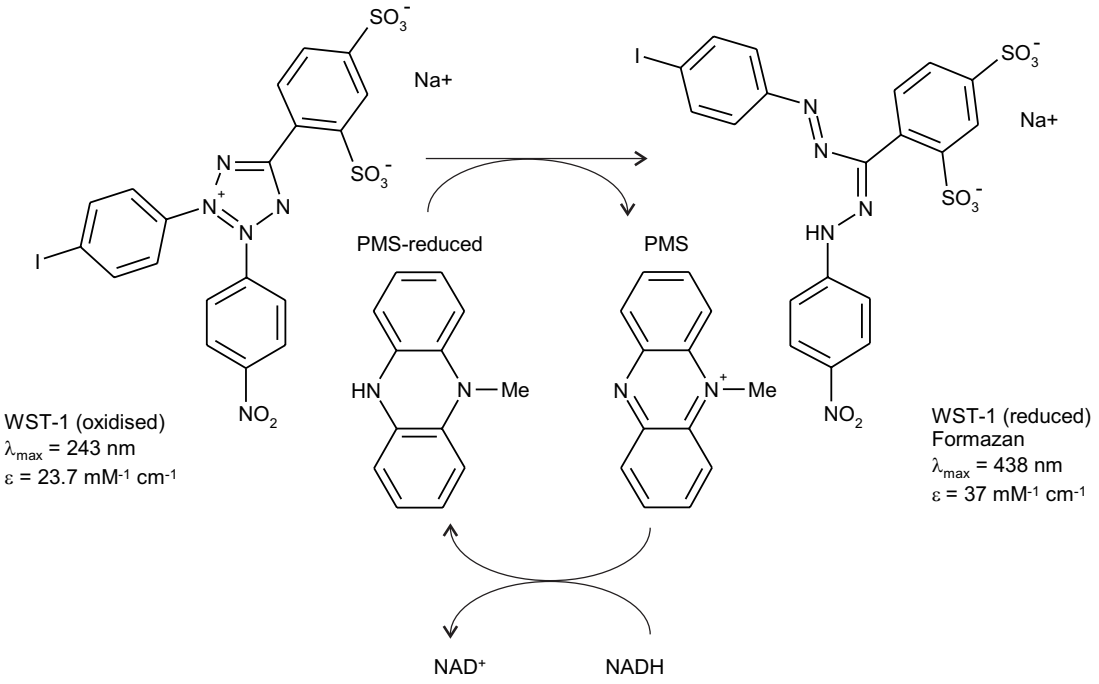

Figure 6.1: Reduction of WST-1 to its reduced form WST-1 formazan by NADH and the intermediate electron acceptor PMS.

Although tetrazolium salts have had a long history of use, the mechanism of their reduction by cellular systems is not well understood (Berridge, *et al.*, 1996). Berridge and colleagues (1993, 1996) have clarified the site of action for some of the tetrazolium salts used in cell proliferation assays, including WST-1. The cell proliferation agent MTT (3-[4,5-dimethylthiazol-2-yl]-2,5-diphenyltetrasodium bromide) is reduced intracellularly to a water insoluble formazan, predominately by NAD(P)H utilising enzymes of the endoplasmic reticulum, within the bone marrow-derived cell line 32D (Berridge and Tan, 1993; Berridge, *et al.*, 1996). New generation water soluble tetrazolium salts, like WST-1, are reduced non-enzymatically to water soluble formazans by NAD(P)H, in the presence of intermediate electron acceptors. Reduction in the presence of whole cells occurs primarily at the cell surface, rather than intracellularly, and has been thought to involve superoxide, since SOD activity inhibits the reduction (Berridge, *et al.*, 1996). Thus, WST-1 reduction is actually a measurement of extracellular membrane redox

activity. In studies with whole cells, WST-1 and its formazan product are found exclusively in the supernatant. Hence, WST-1 is membrane impermeable, consistent with it containing two negatively charged sulfonate groups and the bulky iodophenyl group (Berridge and Tan, 1998).

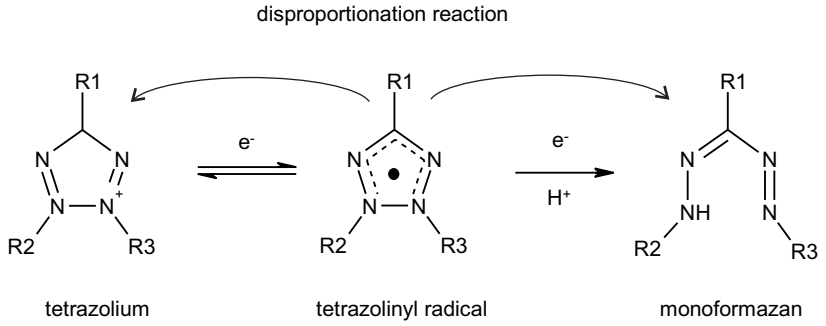

Figure 6.2: Mechanism for reduction of tetrazolium salts.

The reduction of a tetrazolium moiety is a two electron process involving the formation of a tetrazolinyl radical intermediate (Figure 6.2). Tetrazolinyl radical disproportionation yields the progenitor tetrazolium salt and the reduced formazan (Oritani, *et al.*, 2004). These tetrazolinyl radical intermediates can also reduce molecular oxygen to superoxide radicals. In superoxide generating systems such as xanthine oxidase and xanthine (Ukeda, *et al.*, 1999), and xanthine oxidase and hypoxanthine (Peskin and Winterbourn, 2000), WST-1 is reduced by superoxide in a two electron reduction that is inhibited by SOD (Peskin and Winterbourn, 2000).

WST-1 has been applied to the measurement of superoxide formation during the respiratory burst displayed by activated neutrophils (Tan and Berridge, 2000). Neutrophils, when activated by phorbol myristate acetate, effectively reduce WST-1 in the presence and absence of the intermediate electron acceptor 1-methoxy PMS. The measurement of neutrophil superoxide formation by WST-1 can be inhibited almost completely by 20 μg/mL SOD, and by 80% with 10 μM of the NADPH oxidase inhibitor diphenyliodonium (Tan and Berridge, 2000). Glycolytic inhibitors also decrease the extent of WST-1 reduction, suggesting an intracellular origin of reducing equivalents from NADPH (Tan and Berridge, 2000). In contrast, resiniferatoxin, a known inhibitor of membrane NADH oxidase activity (Wolvetang,

et al., 1996), has no effect on the rate of superoxide mediated WST-1 reduction by activated neutrophils (Tan and Berridge, 2000), indicating that the NADPH oxidase and NADH oxidase activities of these cells are distinct.

WST-1 has also been used to study plasma membrane NADH oxidase activity in whole cells (Berridge and Tan, 1998; Berridge and Tan, 2000a, 2000b). Two NADH oxidase activities measurable by WST-1 have been identified; an elutable cell surface NADH oxidase and a transmembrane NADH oxidase. The cell surface NADH oxidase activity was observed in viable cells by reduction of 0.45 mM WST-1 in the presence of 0.2 mM NADH (Berridge and Tan, 2000b). Transmembrane NADH oxidase activity was observed in cells from the Jurkat human T lymphoblastic cell line and other transformed cells by reduction of 0.45 mM WST-1 in the presence of 0.018 mM 1-methoxy PMS (Berridge and Tan, 1998, 2000b). The facilitation of WST-1 reduction by 1-methoxy PMS is thought to occur via the generation of radical species which have a standard redox potential (+80 mV) that is lower than that of NADH (-320 mV) and WST-1 (-120 mV), hence enabling reduction to occur (Tan and Berridge, 2000).

A comparison of WST-1 cell surface and transmembrane activities is shown in the Introduction, Table 1.4. In summary, transmembrane reduction is strongly inhibited by NEM, iodoacetate, capsaicin and SOD, and weakly inhibited by retinoic acid. Reduction is stimulated by cyanide suggesting intracellular NADH concentrations are important for activity. Cell surface reduction is inhibited by pCMBS and SOD and stimulated by NEM, capsaicin, retinoic acid and arachidonic acid. Dicoumarol, which may interfere with ubiquinone cofactor activity in the plasma membrane, also inhibits the transmembrane NADH oxidase activity (Berridge and Tan, 1998, 2000b).

6.2 Motivation

WST-1 reduction at the plasma membrane (WST-1 reductase activity) has been investigated in a number of cell lines, but not in any detail in RBCs. In fact, it has been suggested that RBCs can not reduce WST-1 (Berridge and Tan, 1998). In this Chapter it is shown that WST-1 is reduced at the RBC plasma membrane in the

presence and absence of PMS and this activity is compared to that described by Berridge and Tan (1998, 2000a, 2000b). Spectrophotometric and NMR techniques were used to analyse the rate of reduction and the effects of the reduction on RBC metabolism. WST-1 reduction by RBCs from a number of animal species was also investigated.

6.3 Results

6.3.1 NMR characterisation of WST-1

Neither ^{1}H nor ^{13}C chemical shifts of WST-1 have been published; these were obtained by a combination of 2D NMR techniques. Chemical shifts are expressed relative to TSP, $\delta(^{1}H)$ 0.0, $\delta(^{13}C)$ 0.0, and represent the midpoints of cross-peaks in HSQC and, where applicable, HMBC spectra.

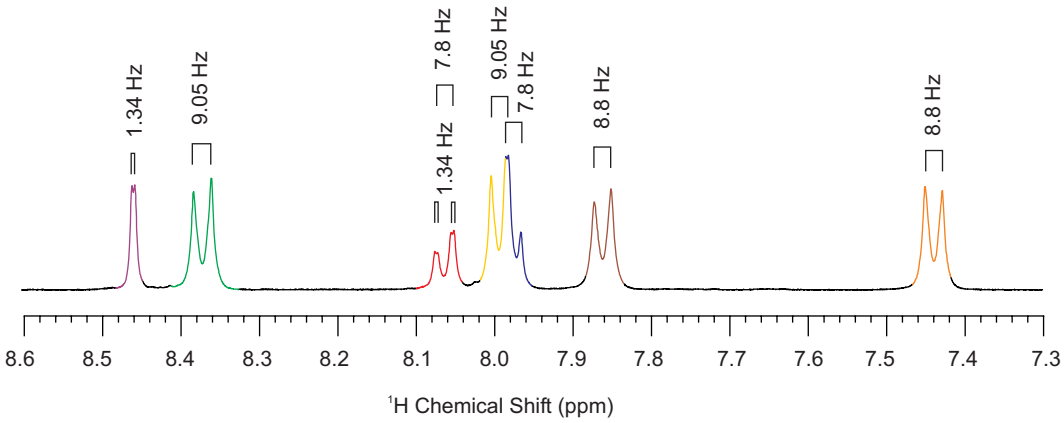

Figure 6.3: ^{1}H NMR spectrum of WST-1 (20 mM in D_2O). Numbers and parentheses indicate *J*-coupling. Peaks arising from protons in different environments are shown in different colours.

The ^{1}H NMR spectrum of WST-1 shows splitting patterns characteristic of *meta* and *ortho* substituted benzene rings (Figure 6.3). For *meta*-protons, spin-spin coupling constants (*J*) are generally in the order of 2-3 Hz, *ortho*-couplings have $J \approx$ 7-10 Hz, and for *para*-couplings $J \approx 1$ Hz (Günther, 1980). Some of the ^{1}H resonances of WST-1 could be assigned directly from the 1D spectrum but, due to resonance overlap, a COSY spectrum (Figure 6.5) was required in order to assign the ^{1}H spectrum completely.

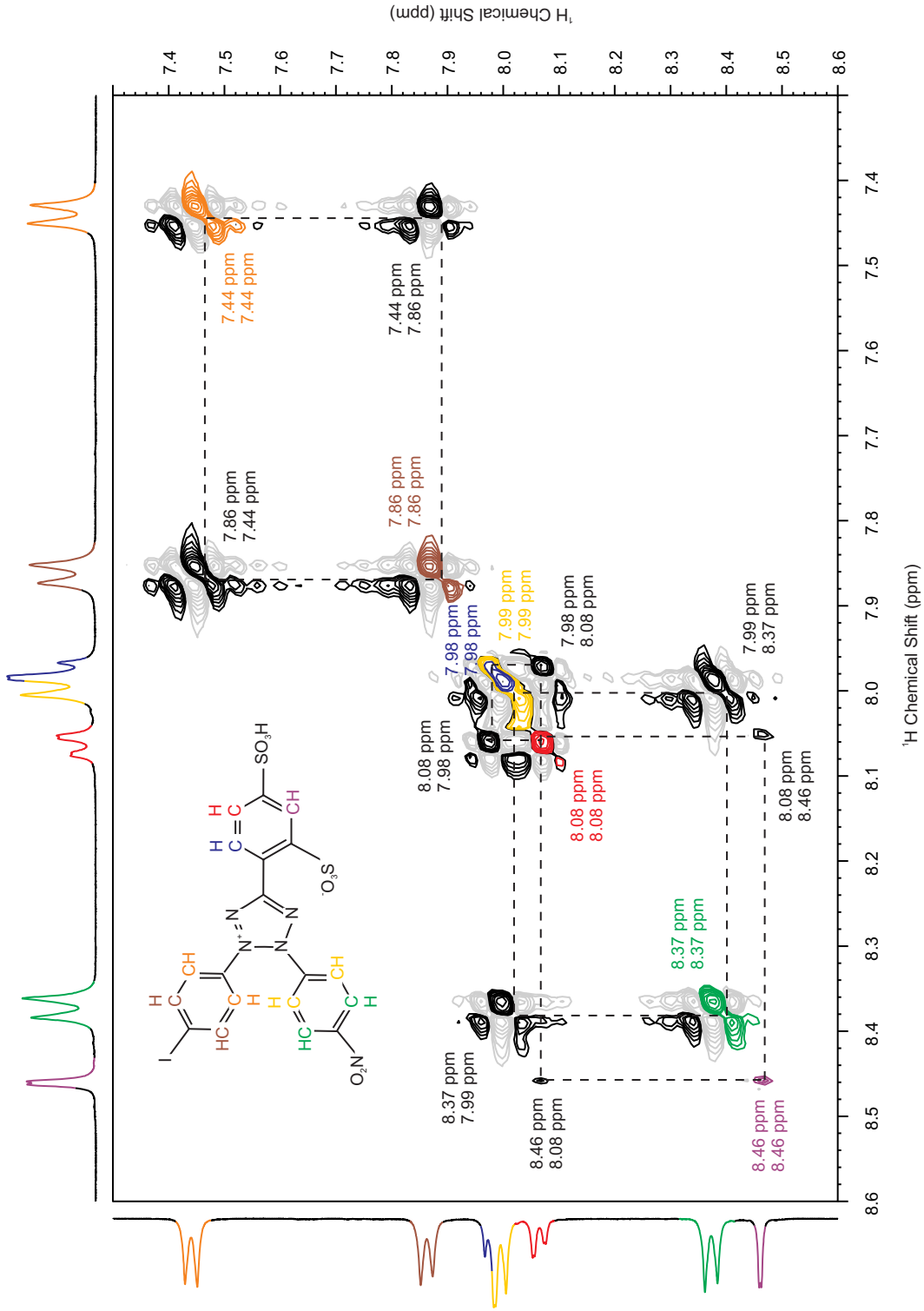

Figure 6.4: ^{1}H double quantum filtered COSY spectrum of 20 mM WST-1 in D_2O. The ^{1}H chemical shifts of the main diagonal and cross-peaks are labelled. The chemical structure of WST-1 is shown for reference. The diagonal peaks are coloured for ease of identification and ^{1}H-^{1}H couplings are identified by the dashed lines. Details of spectral acquisition parameters are described in §2.5.5.

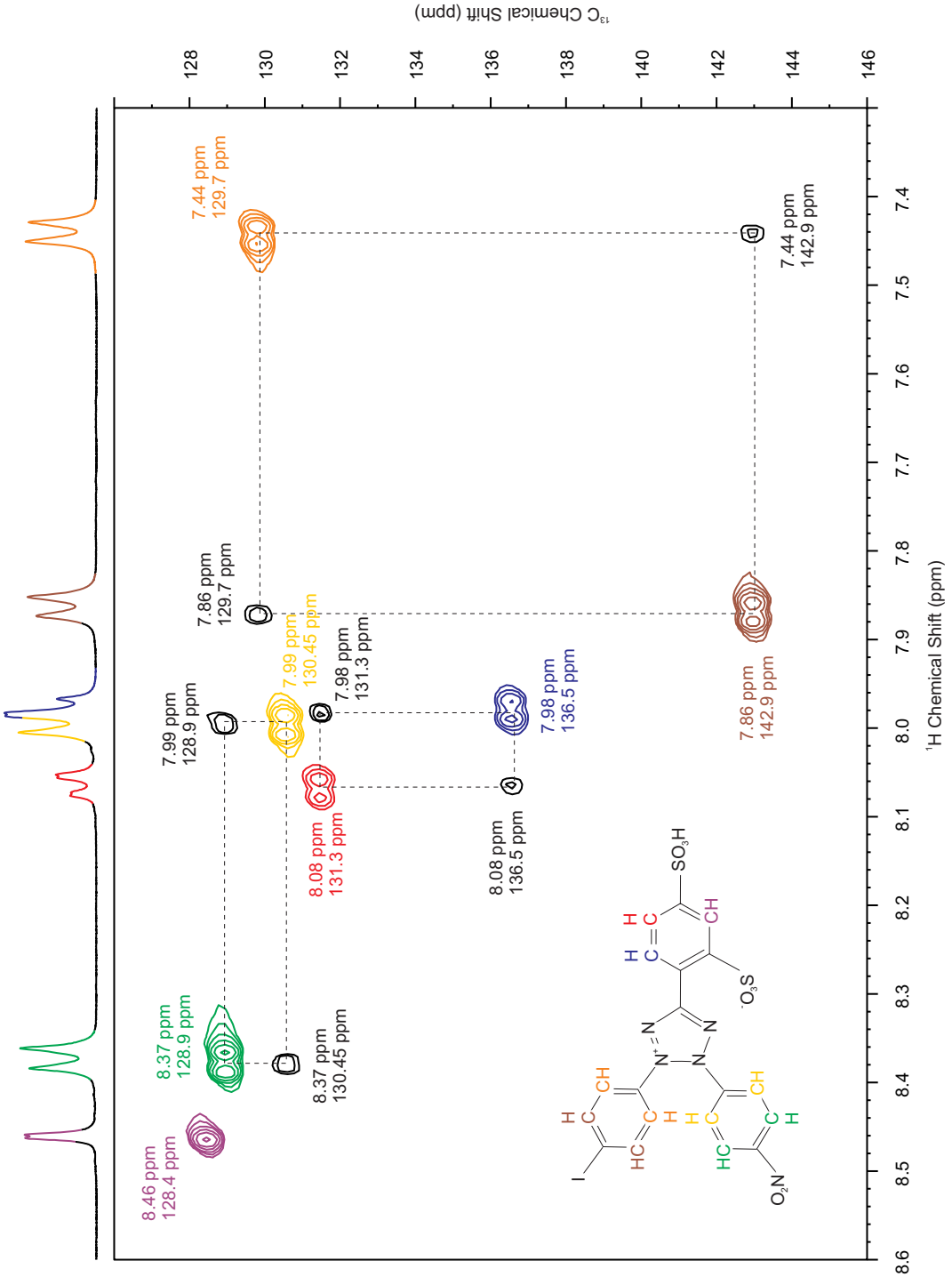

Figure 6.5: ^{1}H-^{13}C HSQC spectrum of 20 mM WST-1 in D_2O. The ^{1}H and ^{13}C chemical shifts of each correlation are coloured for ease of identification. The chemical structure of WST-1 is shown for reference. The uncoloured peaks indicate artefacts that arise from ^{1}H-^{1}H couplings (Turner, *et al.*, 1999). Details of spectral acquisition parameters are given in §2.5.5.

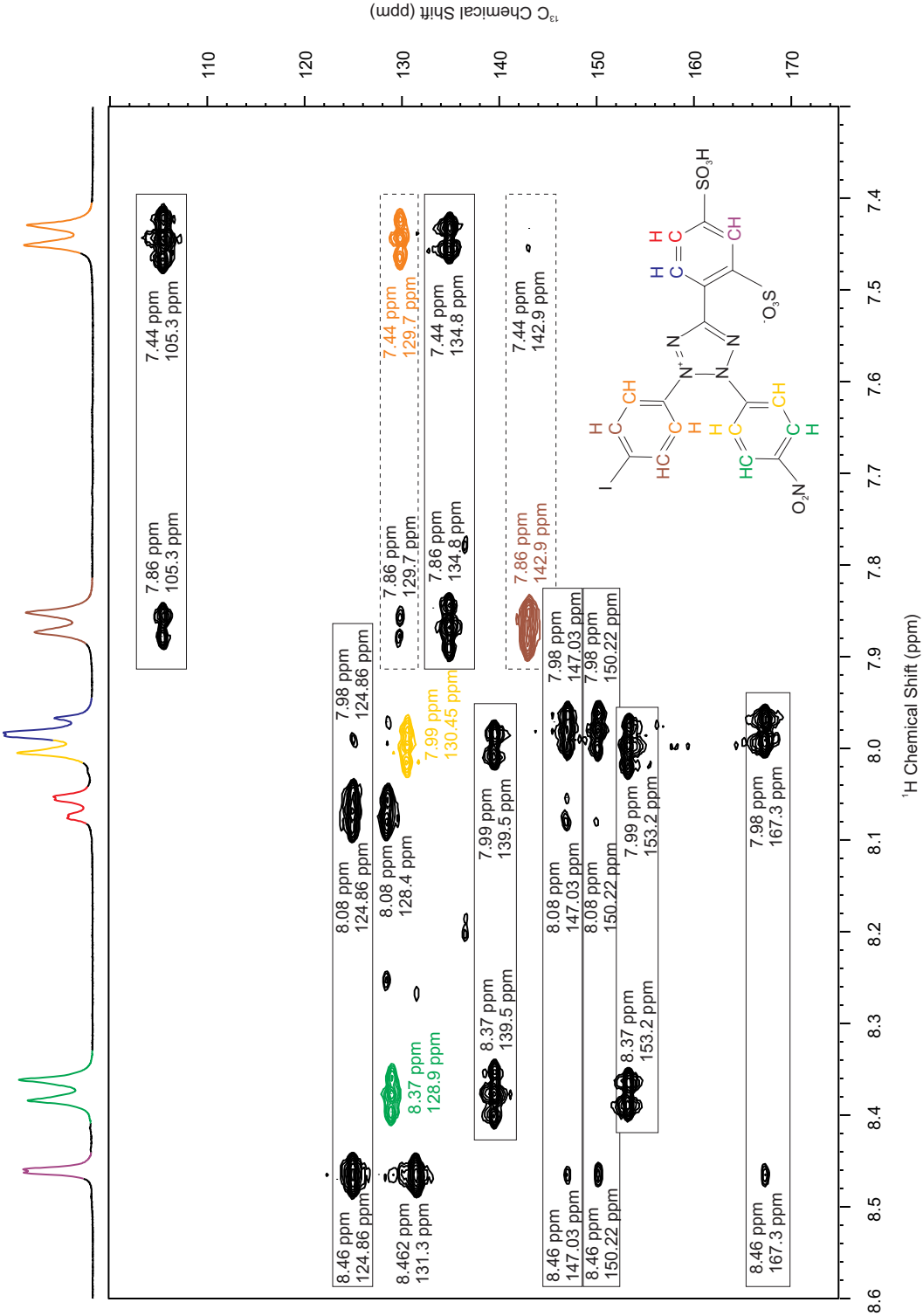

Figure 6.6: ^{1}H-^{13}C HMBC spectrum of 20 mM WST-1 in D_2O. The ^{1}H and ^{13}C chemical shifts of the main correlations are labelled. The chemical structure of WST-1 is shown for reference. Correlations that coincide with those in the HSQC spectrum, and arise here from $^{3}J_{C,H}$ in symmetrical fragments i.e., H-^{12}C-C-^{13}C-(H) are coloured. Correlations to each specific ^{13}C chemical shift are boxed. Details of spectral acquisition parameters are given in §2.5.5.

Correlations in the ^{1}H-^{1}H COSY spectrum (Figure 6.5) of WST-1 identify protons on the same aromatic ring. Thus, the peaks at 8.46 ppm (purple), 8.08 ppm (red), and 7.98 ppm (blue) must be on the disulfonate ring as there are only two different proton environments in the other two rings. The proton and carbon shifts of the disulfonate ring were assigned unequivocally from the COSY (Figure 6.5), HSQC (Figure 6.6) and HMBC (Figure 6.7) spectra. From the correlations in the COSY spectrum, and the splittings in the 1D spectrum, the proton at 8.08 ppm is *meta* to that at 8.46 ppm ($^{4}J_{H,H}$ = 1.34 Hz), and *ortho* to that at 7.98 ppm ($^{3}J_{H,H}$ = 7.8 Hz). The corresponding ^{13}C shifts were obtained from the HSQC spectrum (Figure 6.6). The artefactual cross-peaks due to strong proton-proton couplings (Turner, *et al.*, 1999) are consistent with the COSY-based assignment. Chemical shifts of the quaternary carbons were determined from the HMBC spectrum (Figure 6.7). The evolution delay (80 ms) used for the HMBC experiment optimised magnetisation transfer for $^{n}J_{C,H}$ = 6.25 Hz. Thus, couplings around this value ($^{3}J_{C,H}$ = 7–10 Hz for aromatic protons) have strong correlations, while those much higher or lower ($^{2}J_{C,H}$ = 1–4 Hz for aromatic protons) have weak correlations (Pretsch, *et al.*, 2000). The proton at 8.46 ppm has two strong HMBC correlations (assumed to report $^{3}J_{C,H}$) to 124.9 and 131.3 ppm. The latter can be assigned to C-5 which also has an HSQC correlation, so the 124.8 ppm peak can be assigned to C-1. Similarly, strong HMBC correlations from H-6 identify the two sulfonate bearing carbons and these can be distinguished since H-5 has a stronger ($^{2}J_{C,H}$) correlation to C-4 than to C-2 ($^{4}J_{C,H}$). A strong 3-bond HMBC correlation from H-6 and a weak ($^{4}J_{C,H}$) HMBC correlation from H-3 yields the chemical shift of the single carbon in the heterocyclic ring (167.3 ppm).

The two AA′XX′ systems yield cross-peaks in the HMBC spectrum due to the symmetrical geometry described in the caption of Figure 6.7. Assignment of the iodo- and nitrophenyl rings was based on published data for relative shielding by the substituents (Kalinowski, *et al.*, 1995). The iodo-substituent is more strongly shielding at the *ipso* carbon, while nitro- groups have a larger deshielding effect. Thus, the resonance at 105.3 ppm observed in the HMBC spectra was assigned to the C-4 of the iodophenyl ring and the resonance at 153.2 ppm in HMBC spectra was assigned to the C-4 of the nitrophenyl ring. Following the arguments advanced above, the strongest HMBC correlation at 105.3 ppm is attributed to $^{3}J_{C,H}$ from H-2,6

(7.44 ppm) of the iodophenyl. The nitro-group strongly deshields the protons at the *ortho* position. Hence, H-3,5 of the nitrophenyl ring resonate at 8.37 ppm. In light of the above conclusions the C-1 of the iodo- and nitrophenyl rings can be unequivocally assigned. The complete assignment of WST-1 is shown in Table 6.1.

Table 6.1: Assignment of ^{1}H and ^{13}C chemical shifts for WST-1

	δ(^{1}H)	δ(^{13}C)	Chemical Structure
tetrazolium ring C-5	-	167.3	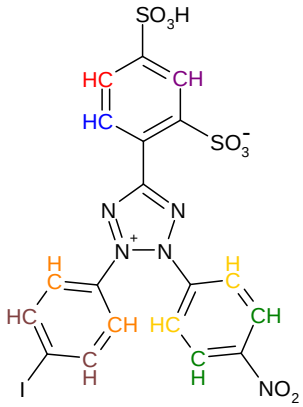
disulfophenyl C-1	-	124.9	
disulfophenyl CSO_3H-2	-	150.2	
disulfophenyl CH-3 (purple)	8.46	128.4	
disulfophenyl CSO_3H-4	-	147.0	
disulfophenyl CH-5 (red)	8.08	131.3	
disulfophenyl CH-6 (blue)	7.98	136.5	
iodophenyl C-1	-	134.8	
iodophenyl CH-2,6 (orange)	7.44	129.7	
iodophenyl CH-3,5 (brown)	7.86	142.9	
iodophenyl CI-4	-	105.3	
nitrophenyl C-1	-	139.5	
nitrophenyl CH-2,6 (yellow)	7.99	130.5	
nitrophenyl CH-3,5 (green)	8.37	128.9	
nitrophenyl CNO_2-4	-	153.2	

6.3.2 Identification of contaminant in commercial WST-1

The ^{1}H NMR spectrum of the WST-1 as supplied by Dojindo (Tokyo, Japan) contained unexpected peaks in the aliphatic region that were likely due to a contaminant whose possible identity was determined by 2D NMR. The COSY, HSQC and HMBC spectra of the contaminant are shown in Figure 6.7. This compound has two groups of coupled protons at 1.86 ppm and 3.75 ppm, and correlated carbons at 27.9 ppm and 70.75 ppm, respectively. The correlations at the same frequencies as HSQC correlations suggest an element of symmetry and thus a cyclical structure. A comparison of the observed carbon chemical shifts with those of 6 membered heterocycles in the literature (Kalinowski, *et al.*, 1995) suggested that the contaminant was 1,4-oxathiane (see Figure 6.7).

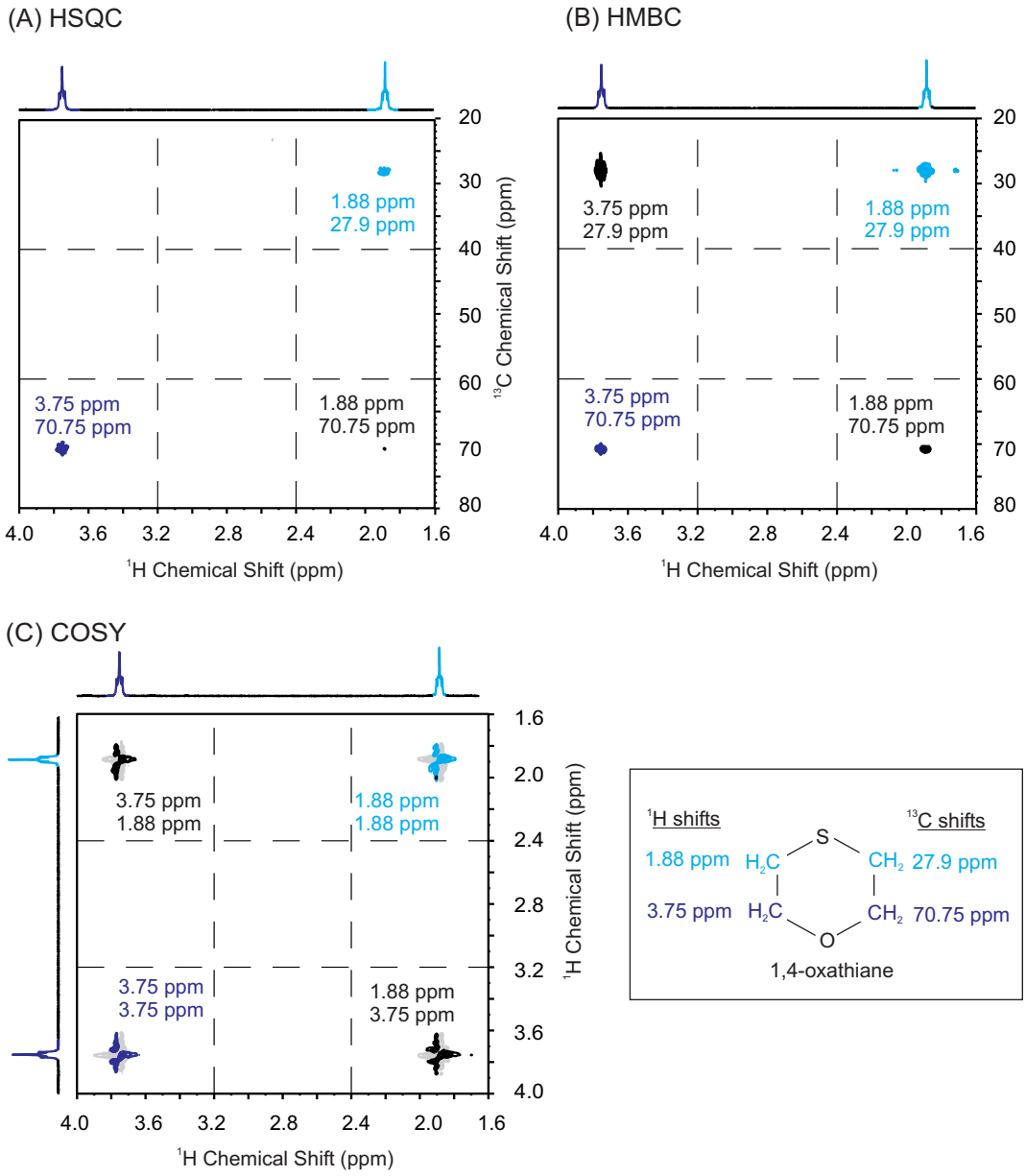

Figure 6.7: (A) HSQC, (B) HMBC and (C) COSY spectra of a contaminant in the WST-1 preparation. The inset shows the structure of the probable contaminant, 1,4-oxathiane, with its ^{1}H and ^{13}C chemical shifts. Details of spectral acquisition are given in §2.5.5.

6.3.3 WST-1 reduction by RBC: ^{1}H NMR studies

Tetrazolium dyes, such as NBT (Dreyer, 1990; Mittler and Zilinskas, 1993; May, *et al.*, 1995b; Ye, *et al.*, 1997; Demehin, *et al.*, 2001; Oritani, *et al.*, 2004) and tetranitroblue tetrazolium (Zurbriggen and Dreyer, 1994; Bulliard, *et al.*, 1997), have previously been used to investigate PMOR and other redox activity. However, due to their low solubility in aqueous solutions and the formation of insoluble formazans

on reduction, they are unsuitable for NMR spectroscopy. PMOR activity has, however, been investigated by ^{13}C NMR with [$^{13}C_6$]ferricyanide as the electron acceptor (Himmelreich and Kuchel, 1997). The iron centre of ferricyanide (Fe^{3+}) is paramagnetic leading to a very broad peak in ^{13}C NMR spectra, while the reduced form, ferrocyanide (Fe^{2+}), is diamagnetic. Hence, the reduction of ferricyanide can be monitored by the appearance of the ferrocyanide resonance at ~180 ppm (Himmelreich and Kuchel, 1997). Although PMOR activity can be measured using [$^{13}C_6$]ferricyanide by ^{13}C NMR, the ^{13}C nucleus is much less sensitive than the ^{1}H nucleus, which has significantly higher natural abundance and gyromagnetic ratio. Hence, a PMOR electron acceptor that is applicable to ^{1}H NMR is desirable. The cellular reduction of WST-1 appears to be an ideal candidate for analysis by ^{1}H NMR spectroscopy: both its oxidised and reduced forms are water soluble, it is not paramagnetic, and its ^{1}H NMR resonances lie between 7–10 ppm while the majority of peaks in a ^{1}H NMR spectrum of RBC are found between 1–4 ppm.

Aqueous solutions of WST-1 have clearly defined peaks in ^{1}H NMR spectra (Figure 6.3), but, surprisingly, no resonances that are clearly identifiable with this molecule were observed in ^{1}H spin-echo NMR spectra (τ = 60 ms) of human RBC suspensions to which WST-1 was added (Figure 6.8).

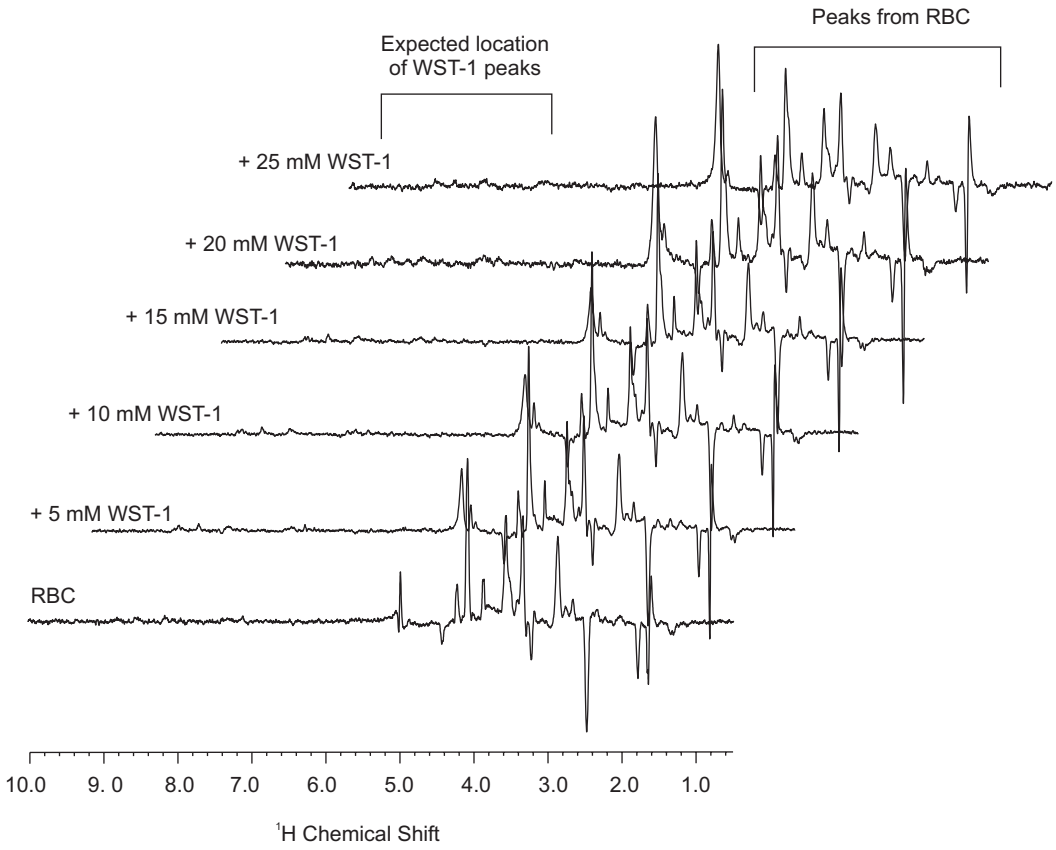

Figure 6.8: ^{1}H spin-echo (τ = 60 ms) NMR spectra of WST-1 in RBC suspensions. WST-1 at increasing concentrations was added to RBC suspensions (Hc = 0.65) in 50 mM PBS (in D_2O) and ^{1}H spin-echo (τ = 60 ms) NMR spectra acquired. All spectra were acquired on a Bruker DRX-400 spectrometer at 37 °C. Details of spectral acquisition parameters are given in §2.5.6.

To investigate the basis of the loss of signal the spin-echo delay time was shortened to 20 ms (Figure 6.9). Decreasing the delay time reduces signal loss due to spin-spin relaxation and changes the relative phase modulation of the peaks; it also allows the refocusing of some of the magnetisation from large molecules. The resolution of peaks in the aromatic region of the spectrum improved but, as the majority of these peaks were also observed in the control RBC suspension, they were most likely to have arisen from Hb histidine residues and not WST-1. To determine whether the absence of WST-1 signals was due to coupling effects, a CPMG pulse sequence was applied. However, as with the other pulse sequences investigated, WST-1 peaks were still not clearly identifiable in RBC suspensions (Figure 6.10).

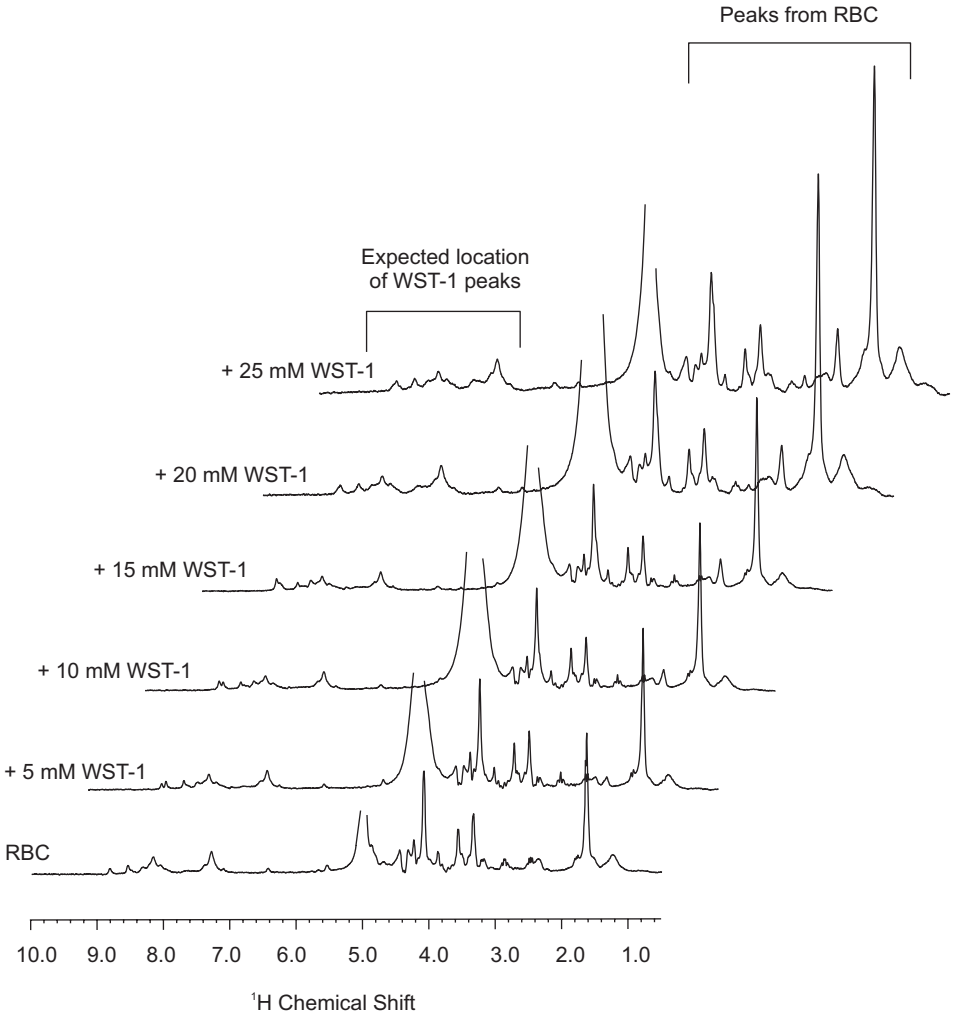

Figure 6.9: ^{1}H spin-echo (τ = 20 ms) NMR spectra of WST-1 in RBC suspension. WST-1 was added to RBC suspensions (Hc = 0.65) in 50 mM PBS (in D_2O) in increasing concentrations and ^{1}H spin-echo (τ = 20 ms) NMR spectra were acquired. All spectra were acquired on a Bruker DRX-400 spectrometer at 37 °C. Details of spectral acquisition parameters are given in §2.5.6.

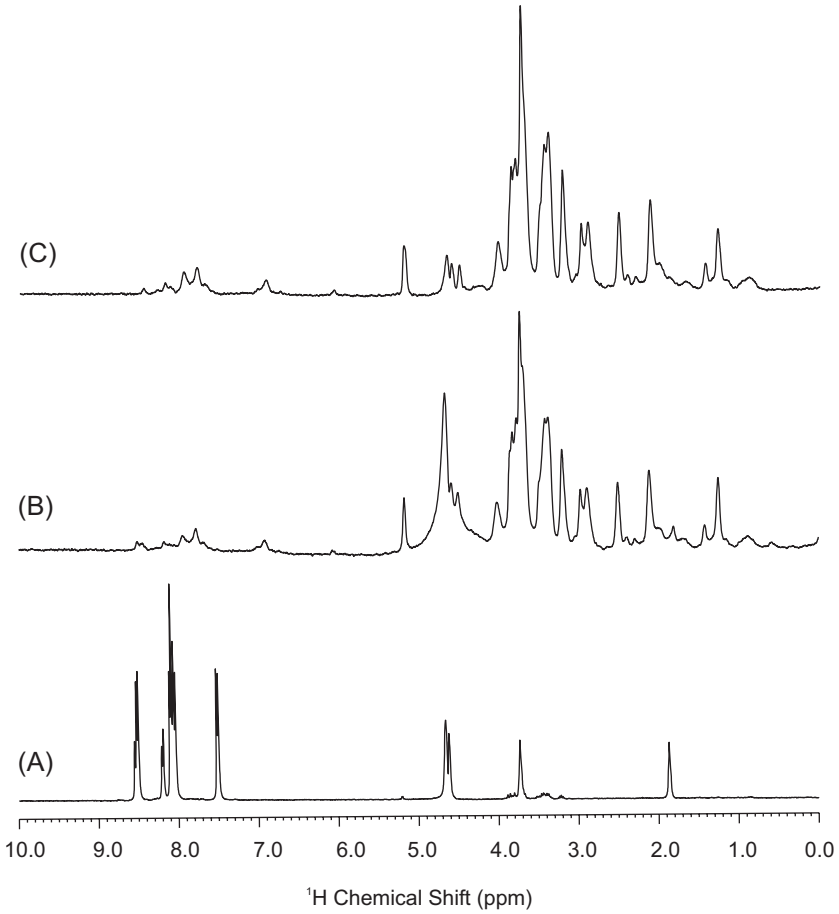

Figure 6.10: CPMG spin-echo spectra of: (A) 5 mM WST-1 in D_2O; (B) 5 mM WST-1 in an RBC suspension, Hc = 0.65, in 50 mM PBS/D_2O; (C) RBC suspension, Hc = 0.65, in 50 mM PBS (in D_2O). All spectra were acquired on a Bruker DRX-400 spectrometer at 37 °C. Details of spectral acquisition parameters are given in §2.5.6.

The working hypothesis for the reduction of WST-1 is that it occurs at the plasma membrane. Therefore, it is likely that WST-1 interacts with the plasma membrane and/or proteins in the membrane. The spin-echo pulse sequences employed only refocus magnetisation from small molecules which relax slowly. Therefore, large molecules or molecular structures such as proteins and membranes which relax much more rapidly are not observed in spin-echo spectra. If a small molecule, such as WST-1, is bound for an appreciable period on a protein or the membrane, then its relaxation is enhanced and its magnetisation may not be observed in these experiments. ^{1}H-CPMG spectra of WST-1 added to a suspension of BSA clearly show peaks from the 1,4-oxathiane contaminant in the WST-1 preparation but not

resonances from WST-1 itself (Figure 6.11). Hence, WST-1 appears to bind to proteins (and potentially membranes) within the time frame of the NMR experiment.

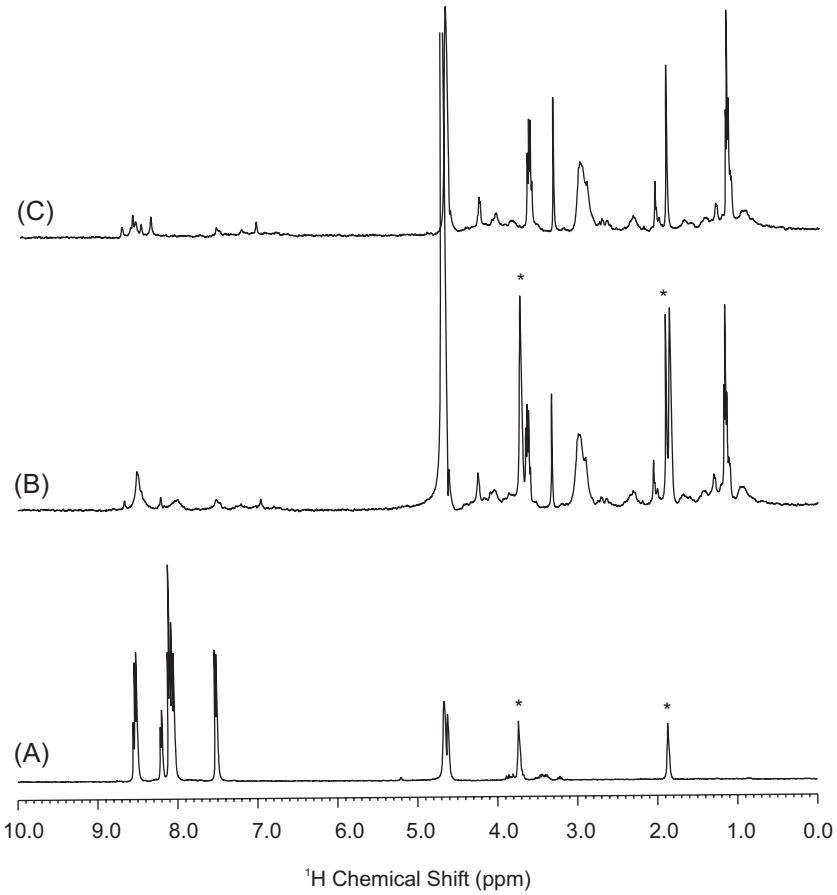

Figure 6.11: CPMG spin-echo spectra of: (A) 5 mM WST-1 in D_2O; (B) 5 mM WST-1 in 2.5% BSA in D_2O; (C) 2.5% BSA in D_2O. The * denote peaks from the contaminant, 1,4-oxathiane, that is present in the commercial WST-1 preparation. All spectra were acquired on a Bruker DRX-400 spectrometer at 37 °C. Details of spectral acquisition parameters are given in §2.5.6.

Unfortunately, it would appear that WST-1 reduction by RBC suspensions can not be monitored using ^{1}H NMR spectroscopy. However, the effects of WST-1 reduction on RBC metabolism are measurable and are discussed in §6.3.6.

6.3.4 The reduction of WST-1 and adaptation of measurements to microtitre plate format

The WST-1 reductase assay is based on the colour change which occurs when WST-1 is reduced to its yellow formazan (Figure 6.1). Due to the high solubility and

extinction coefficient (37 $mM^{-1}cm^{-1}$) of WST-1, the assay of WST-1 reduction is readily adapted to microtitre plate format (Berridge and Tan, 1998; Peskin and Winterbourn, 2000; Tan and Berridge, 2000). The absorbance of WST-1 formazan at 450 nm, a common wavelength filter of microtitre plate readers, is within 5% of the peak height at the λ_{max} (438 nm). Hence, the sensitivity of the spectrophotometric assay should be maintained upon conversion to the microtitre-plate format (Peskin and Winterbourn, 2000).

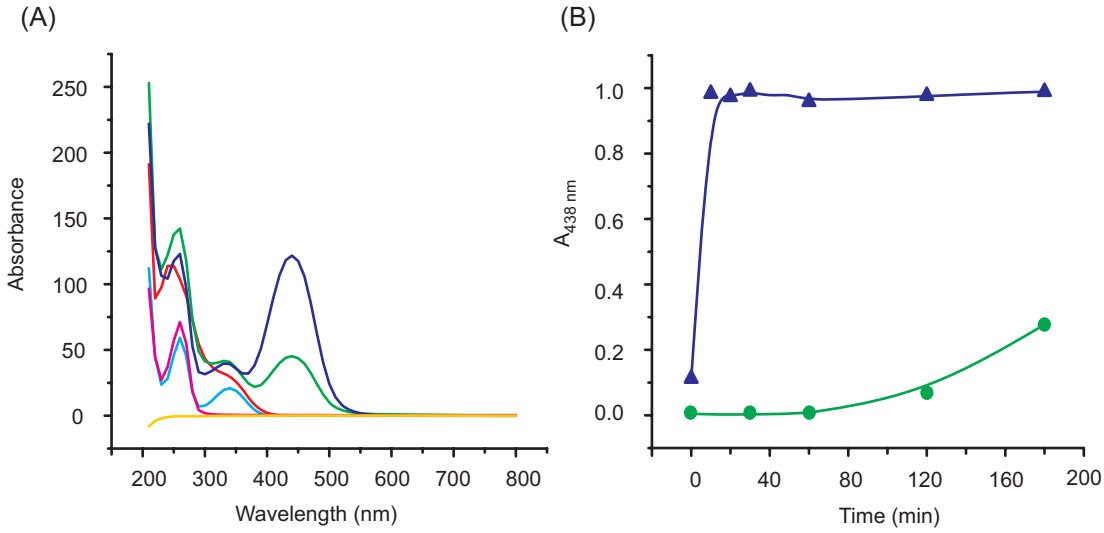

Figure 6.12: Absorbance spectra of WST-1, NADH and PMS (A) and time dependence of WST-1 reduction (B). (A) 5 mM WST-1 (—); 5 mM WST-1 and 5 mM NADH (—); 5 mM WST-1, 5 mM NADH and 5 µM PMS (—), 5 mM NADH (—), 5 mM NADH and 5 µM PMS (—); and 5 µM PMS (—), were incubated for 3 h in 2 mM PBS, pH 7.4, at 37 °C prior to acquisition of absorption spectra. **(B)** Time dependence of 5 mM WST-1 reduction by 5 mM NADH (●), and 5 mM NADH and 5 µM PMS (▲).

WST-1 formazan was produced by incubating WST-1 with NADH in the presence of the intermediate electron acceptor PMS (Figure 6.12B). As shown in Figure 6.12A, the absorption spectrum of WST-1 is characterised by a peak at ~240 nm and a shoulder at ~330nm; the absorption spectrum of NADH has peaks at 260 nm and 340 nm. PMS, at the concentrations used in these experiments, did not show any absorbance above baseline levels. When incubated alone, WST-1 and NADH react slowly with approximately 20% of the WST-1 reduced after three hours (Figure 6.12B). In contrast, addition of PMS to the reaction mixture resulted in immediate reduction of WST-1, although it only resulted in 70% conversion for the 3h time

period (Figure 6.12B). In the absence of WST-1, NADH is oxidised by PMS. These results are consistent with PMS acting as an electron shuttle between NADH and WST-1 (Tan and Berridge, 2000).

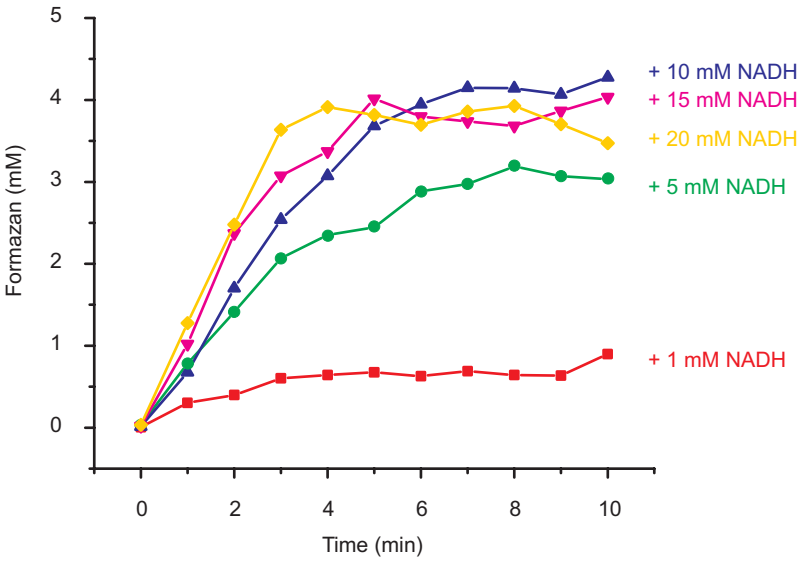

Figure 6.13: Dependence of WST-1 formazan formation on NADH concentration. 5 mM WST-1, 5 µM PMS and increasing concentrations of NADH (1–20 mM) were incubated at 25 °C for 10 min and the formation of WST-1 formazan assayed.

The rate and extent of reduction of WST-1 by NADH (in the presence of PMS) is dependent on the concentration of NADH. At 1 mM NADH, limited reduction of 5 mM WST-1 occurred at pH 7.4 (Figure 6.13). The rate and extent of WST-1 reduction increased with increasing NADH concentrations up to 10 mM. Above this concentration, the reaction appeared to have reached completion, with 90% of the WST-1 in the reduced form. Additionally, the pH optimum for this reaction is reported to be 8.5. Hence, at pH 7.4 complete conversion may not occur (Ishiyama, *et al.*, 1993). The concentration dependence of WST-1 reduction on PMS was not investigated.

For calibration of microtitre plate WST-1 assays, a formazan standard curve (Figure 6.14) was developed. The amount of formazan (nmol) has a linear relationship with the absorbance at 450 nm over the concentration range 0–10 nmol formazan per well (0–100 µM formazan, 100 µl per well, pathlength ~3.3 mm). The microtitre plate adjusted calibration factor (ε_{eff}) for WST-1 formazan was taken as 0.093 $nmol^{-1}$ and

was used to calculate the concentration of formazan produced (mmol (L RBC)$^{-1}$) in cellular assays (§2.4.7).

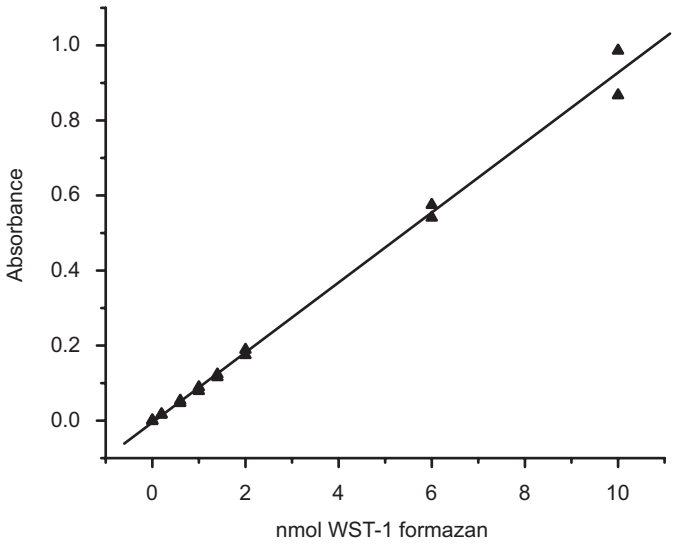

Figure 6.14: WST-1 formazan calibration curve for microtitre plate reader using a 450 nm wavelength filter. Formazan was made by incubating 5 mM WST-1, 5 μM PMS and 10 mM NADH in 2 mM PBS, pH 7.4 for 10 min at 25 °C, and the concentration determined by measuring the absorbance at λ = 438 nm. The yield of formazan was then used to generate the above data which were fitted by linear regression. The relationship between absorbance and nmol formazan was: Abs = 0.093 × (nmol formazan) – 0.005.

6.3.5 WST-1 reductase activity in RBC suspensions

In previous applications of microtitre plate protocols investigating WST-1 reduction, cells were placed in the wells of the plate and the formation of formazan measured directly by spectrophotometry (Berridge and Tan, 1998, 2000b; Tan and Berridge, 2000). With RBCs this technique is complicated by the fact that Hb absorbs strongly at 450 nm making it virtually impossible to measure changes in absorbance due to formazan formation. In fact, it is also difficult to measure WST-1 reductase activity in haemolysates even when low concentrations of RBCs are used. However, as WST-1 and its formazan product are known to be membrane impermeable (Berridge and Tan, 1998), removal of the supernatant from the cells and assay of the supernatant fraction enable the extent of reduction to be measured (see §2.4.7). RBC controls in the absence of WST-1 accounted for the absorbance at 450 nm due to haemolysis. Neither WST-1 nor PMS alone or in combination appeared to induce haemolysis.

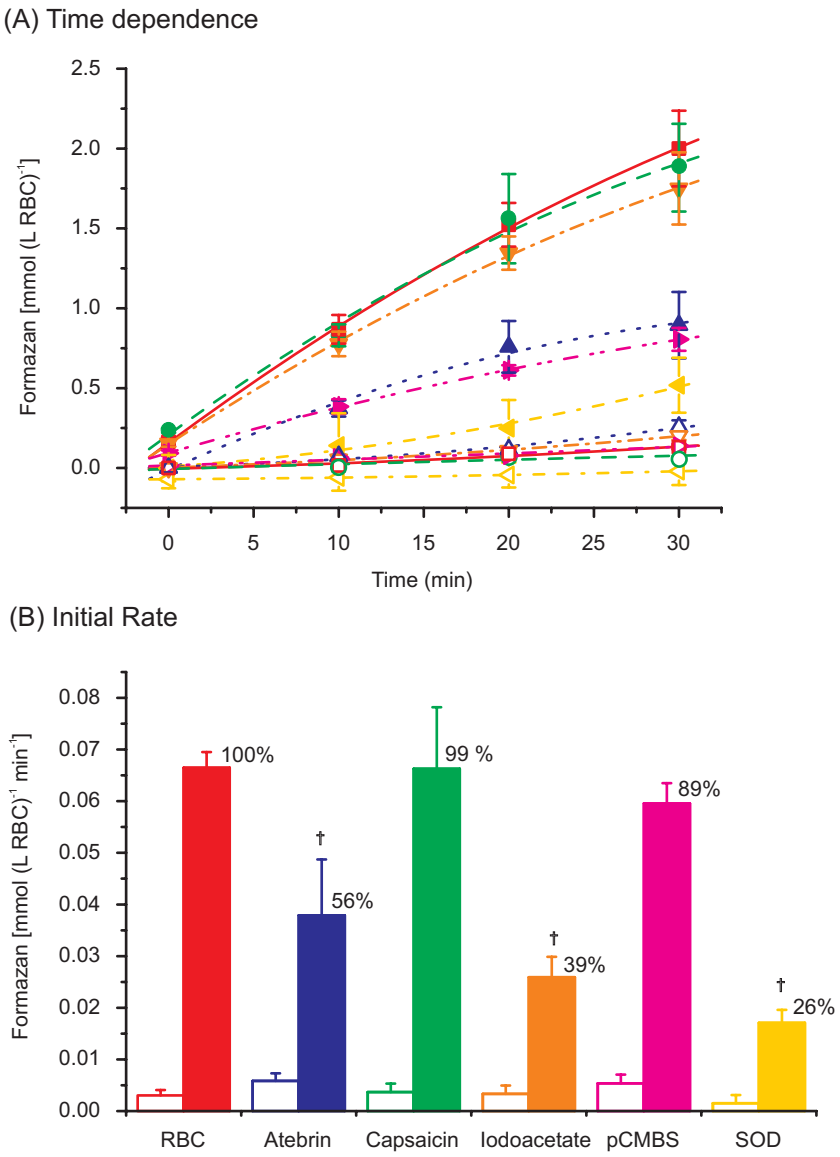

Figure 6.15: Effect of PMOR inhibitors on WST-1 reductase activity. RBCs in 2 mM PBS containing 5 mM glucose were incubated at 37 °C for 30 min with 5 mM WST-1 (open symbols and bars), and 5 mM WST-1 and 5 µM PMS (closed symbols and bars) in the presence of no inhibitors (■), 1 mM atebrin (▲), 200 µM capsaicin (●), 1 mM iodoacetate (▶), 1 mM pCMBS (▼), and 20 µg/mL SOD (◀). **(A)** Time dependence of formazan formation, and **(B)** rate of formazan formation over the first 20 min. Data points were the average of at least five experiments performed on separate blood samples; error bars denote ± 1 s.d. All data were adjusted for background absorbance due to haemolysis, prior to calculating the WST-1 formazan concentration. Percentages **(B)** indicate relative WST-1 + PMS rate; data were analysed with the non-parametric Mann-Whitney U test for statistically significant differences from the rate observed with WST-1 and PMS; † denote rates which had $p < 0.05$ relative to the control.

The rate of WST-1 reduction was linear over the first 20 min (Figure 6.15A) and was increased ~23 fold by the presence of PMS. The rate of WST-1 reduction was inhibited by 1 mM atebrin, 1 mM iodoacetate and 20 μg/mL SOD and unaffected by 200 μM capsaicin or 1 mM pCMBS (Figure 6.15B). Atebrin had slightly different effects on WST-1 alone, with an apparent increase in the rate of reduction. Atebrin was also found to form a flocculum when added to a solution of WST-1.

6.3.6 Effect of WST-1 reduction on RBC metabolism

^{1}H spin-echo NMR experiments on glucose-supplied RBCs indicated that over a 3 h period glutathione was gradually oxidised. The inclusion of WST-1 in the extracellular medium slightly decreased the initial rate of GSH oxidation compared to control RBCs. However, the addition of both WST-1 and PMS resulted in a marked increase in the rate and extent of GSH oxidation compared to controls (Figure 6.16).

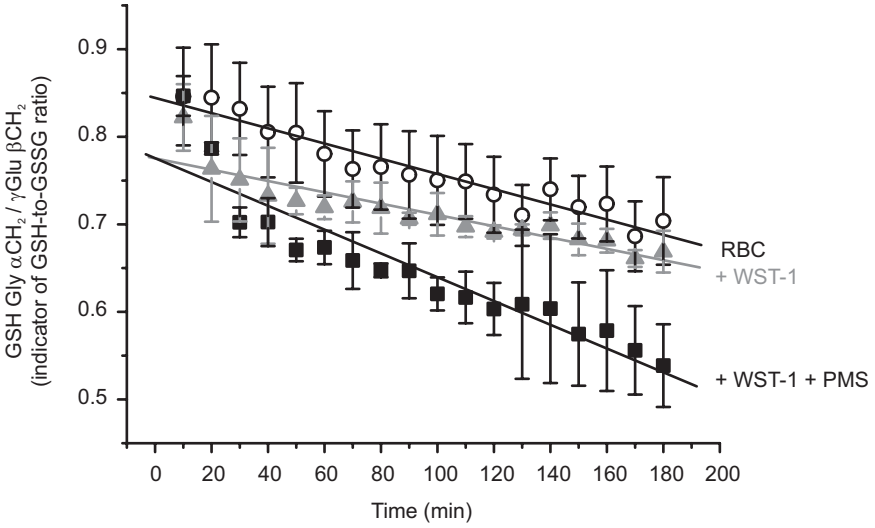

Figure 6.16: Effect of WST-1 on the intracellular reduced-to-oxidised glutathione ratio. RBCs, Hc = 0.65, in 2 mM PBS (10% D_2O) containing 5 mM glucose were incubated at 37 °C with no additions (○), 5 mM WST-1 (▲), and 5 mM WST-1 plus 5 μM PMS (■). ^{1}H spin-echo NMR spectra (τ = 60 ms) were acquired at 10 min intervals over 3 h. The relative change in the GSH-to-GSSG ratio was determined by dividing the integral of the Gly αCH_2 resonance by that of the γGlu βCH_2 resonance. Lines of best fit are shown. The rates of decrease in the GSH-to-GSSG ratio per min were 8.63×10^{-4}, 6.45×10^{-4}, and 13.6×10^{-4} for RBC controls, with WST-1, and with both WST-1 and PMS, respectively. Data points represent the average of three separate experiments with error bars denoting ± 1 s.d.

^{1}H spin-echo NMR experiments on glucose-supplied RBCs indicated that over a 3 h period lactate was the end product of glycolysis, with the LDH reaction reaching equilibrium after 1.5 h. The inclusion of WST-1 in the extracellular medium decreased the metabolic rate, with a much lower lactate-to-pyruvate ratio reflecting an increase in the concentration of pyruvate (Figure 6.17). The addition of both WST-1 and PMS decreased the metabolic rate to a greater extent than the addition of WST-1 alone.

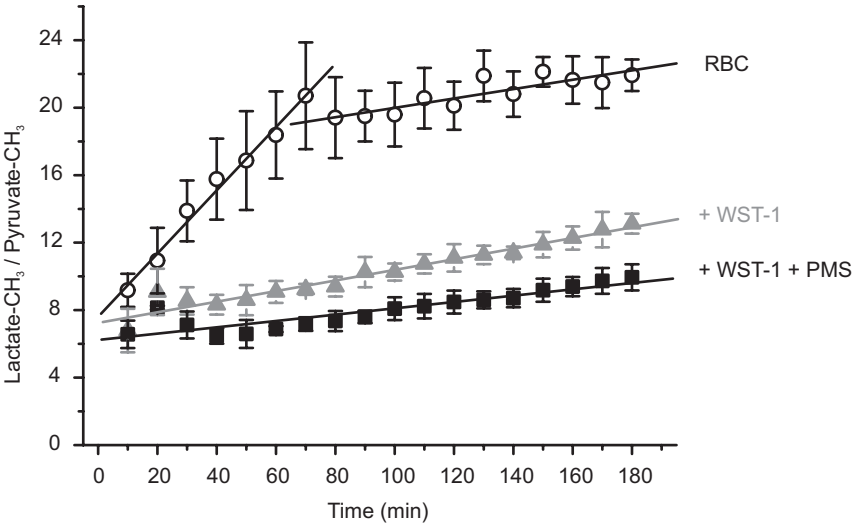

Figure 6.17: Effect of extracellular WST-1 on the metabolic rate. RBCs, Hc = 0.65, in 2 mM PBS (10% D_2O) containing 5 mM glucose were incubated at 37 °C with no additions (○), 5 mM WST-1 (▲), and 5 mM WST-1 plus 5 μM PMS (■). ^{1}H spin-echo NMR spectra (τ = 60 ms) were acquired at 10 min intervals over 3 h. The relative change in the lactate-to-pyruvate ratio was determined by dividing the integral of the lactate-CH_3 peak by that of the pyruvate-CH_3 peak. Lines of best fit are shown. The rates of increase in the lactate-to-pyruvate ratio per min were initially 0.187 and finally 0.028 for the RBC control, 0.031 in the presence of WST-1 and 0.019 in the presence of both WST-1 and PMS. Data points represent the average of three separate experiments with error bars denoting ± 1 s.d.

6.3.7 WST-1 reduction by RBC from various mammalian species

The RBC WST-1 reduction rate (± PMS) varied when investigated with RBCs from different animal species. The rate of reduction was highest for human and sheep

RBCs, then cattle and horse RBCs. Kangaroo RBCs exhibited limited WST-1 reductase activity (± PMS), and also displayed high levels of haemolysis (Figure 6.18).

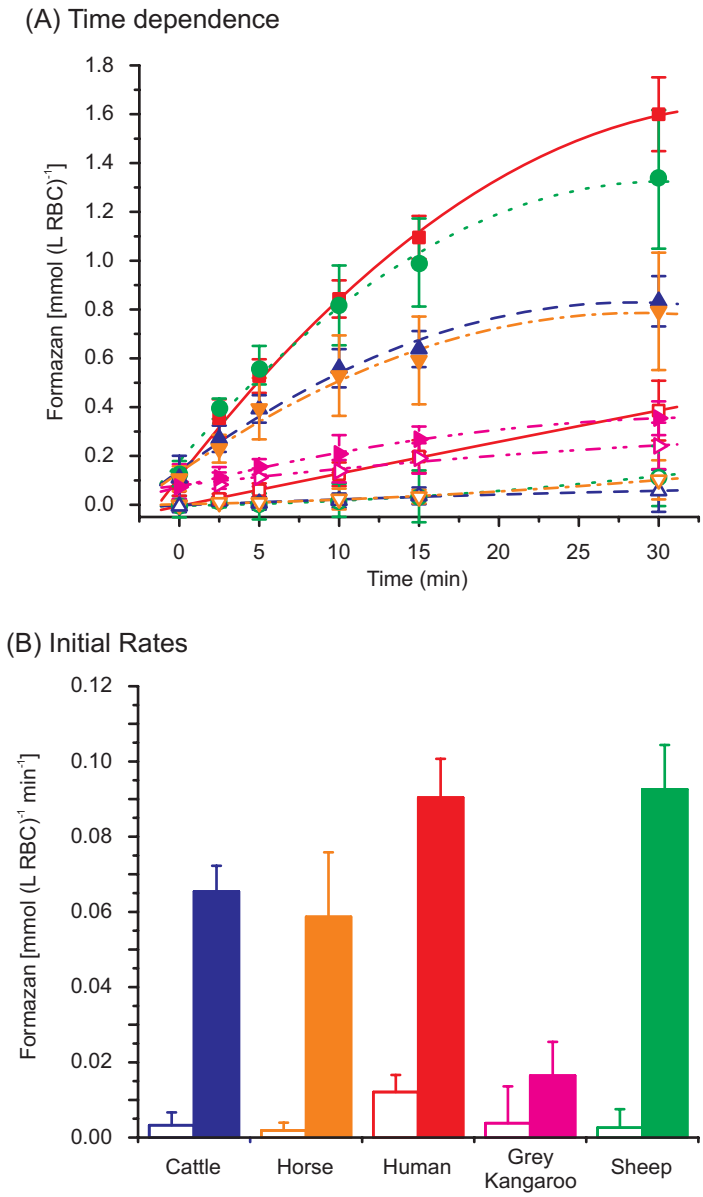

Figure 6.18: WST-1 reductase activity by RBC from different animal species. RBC from cattle (▲, n = 6), horse (▼, n = 7), human (▼, n = 6), grey kangaroo (▶, n = 4), and sheep (●, n = 8) were incubated in 2 mM PBS containing 5 mM glucose at 37 °C for 30 min with 5 mM WST-1 (open symbols and bars), or 5 mM WST-1 and 5 µM PMS (closed symbols and bars). **(A)** Time dependence of formazan formation, and **(B)** rate of formazan formation over first 10 min. Data points are the average of experiments performed on blood from a number (n) of different individuals within the species. Error bars denote ± 1 s.d. All data were adjusted for background absorbance due to Hb prior to calculating the WST-1 formazan concentration.

6.4 Discussion

WST-1, in the absence of cells, was reduced slowly by NADH and rapidly by a combination of NADH and PMS (Figure 6.12B). The rapid reduction in the presence of both NADH and PMS was dependent on the NADH concentration (Figure 6.13). Whilst at low NADH concentrations the reduction was very slow, reduction occurred more rapidly as the concentration was increased and reached 90% completion within 5 min (Figure 6.13). Reduction of WST-1 was not achieved with PMS alone. Thus, NADH appears to be responsible for the formation of the tetrazolinyl radicals and, hence, the reduction of WST-1 in the absence of cells.

In RBC suspensions, however, WST-1 was reduced in both the presence and absence of PMS, without the need for supplemental NADH. WST-1 was also reduced more rapidly by RBCs in the presence of NADH than in the absence of cells, and at a rate comparable to that with PMS (data not shown). WST-1 reduction rates for RBC were 3.04 ± 1.03 μmol $(L\ RBC)^{-1}\ min^{-1}$ and, in the presence of PMS, 66.5 ± 3 μmol $(L\ RBC)^{-1}min^{-1}$ (Figure 6.15).

Trans-membrane NADH oxidase activity has been investigated in a number of cell lines using WST-1 and PMS. The rate of reduction of WST-1 appears to depend on the cell line used and does not correlate with the cell surface NADH oxidase activity (Berridge and Tan, 2000a). Transmembrane NADH oxidase reduction rates range from those observed in resting neutrophils, 0.4 ± 0.2, to those observed in $143B\rho^0$ osteosarcoma cells, 45.6 ± 5.8 $mA_{450}\ min^{-1}$ $(3 \times 10^5\ cells)^{-1}\ mL^{-1}$ (Berridge and Tan, 2000a). Cell surface reduction rates (measured with WST-1 and NADH) are generally lower, and lie between 1.45 ± 0.43 and 10.59 ± 0.30 $mA_{450}\ min^{-1}$ $(5 \times 10^5\ cells)^{-1}\ mL^{-1}$, for resting neutrophils and Malme 3M melanoma cells, respectively (Berridge and Tan, 2000a). Expressed in the same units, the rates of WST-1 reduction by RBCs, in the absence and presence of PMS, are 0.34 ± 0.11 and 4.53 ± 0.6 $mA_{450}\ min^{-1}$ $(4 \times 10^9\ cells)^{-1}\ mL^{-1}$, respectively. Hence, even in the presence of PMS, the rate of WST-1 reduction by RBCs is significantly lower than that observed for transformed and non-transformed cell lines.

The WST-1 reductase activity observed in the plasma membrane of RBCs displays many similarities to the transmembrane NADH oxidase activity reported by Berridge and Tan (1998, 2000a, 2000b). WST-1 reduction was inhibited by SOD, iodoacetate and atebrin, while pCMBS had no effect (Figure 6.15). pCMBS, a cell impermeable thiol-blocking agent, has previously been reported to have no effect on transmembrane NADH oxidase activity (i.e., PMS mediated WST-1 reduction), while having an inhibitory effect on cell surface NADH oxidase activity (i.e., NADH mediated WST-1 reduction) (Berridge and Tan, 1998; Berridge and Tan, 2000a, 2000b). Thus it appears that the PMS-mediated WST-1 reduction noted in this study for RBCs is a transmembrane, rather than cell surface, NADH oxidase activity.

Capsaicin did not inhibit WST-1 reduction by RBC suspensions. Varied effects of capsaicin on NADH oxidase activity have been reported. Capsaicin has been reported to inhibit NADH oxidase activity in the isolated membranes of transformed cells but not the NADH oxidase activity of non-transformed cells (Morré, *et al.*, 1995). However, the transmembrane NADH oxidase activity in whole cells of both non-transformed growth-factor dependent cell lines and transformed cell lines, measured with WST-1, are inhibited by capsaicin (Berridge and Tan, 1998, 2000b).

Atebrin a known inhibitor of transmembrane ferricyanide reduction (Löw and Crane, 1995) also appeared to inhibit PMS-mediated WST-1 reduction (Figure 6.15). However, it was noted that atebrin and WST-1 formed a floc when mixed together. Therefore the noted inhibitory effect of atebrin may have been caused by a decreased effective concentration of WST-1 in the cell suspension rather than atebrin acting as a *bona fide* inhibitor of the membrane reductase activity.

SOD has also been shown to inhibit the RBC mediated reduction of WST-1, suggesting the involvement of superoxide ($O_2^{\cdot -}$) in the reaction, although a caveat should be noted (Fridovich, 1997). Specifically, it has been suggested that SOD inhibition of WST-1 reduction is due to the mechanism outlined in Eqn 6.1–6.4 (Baker, *et al.*, 2004a): WST-1 is initially reduced to the tetrazolinyl radical intermediate (WST-1H*;Eqn 6.1). The radical either disproportionates to WST-1

formazan ($WST\text{-}1H_2$) and oxidised WST-1 (Eqn 6.2), or it reacts with molecular oxygen forming oxidised WST-1 and superoxide (Eqn 6.3). SOD converts superoxide into hydrogen peroxide (Eqn 6.4) which drives Eqn 6.3 to the right, resulting in the tetrazolinyl radical taking the path of Eqn 6.3 rather than Eqn 6.2, limiting the formation of the formazan product (Baker, *et al.*, 2004a).

$$WST\text{-}1 + e^- + H^+ \longrightarrow WST\text{-}1H^* \quad (6.1)$$

$$WST\text{-}1H^* + WST\text{-}1H^* \longrightarrow WST\text{-}1 + WST\text{-}1H_2 \quad (6.2)$$

$$WST\text{-}1H^* + O_2 \rightleftharpoons WST\text{-}1 + O_2^{*-} \quad (6.3)$$

$$O_2^{*-} + O_2^{*-} + H^+ \xrightarrow{SOD} 2H_2O_2 \quad (6.4)$$

Thus, although SOD substantially inhibited (74%) the reduction of WST-1 at the RBC plasma membrane, the exact contribution of superoxide in the reduction of WST-1 was not determined.

WST-1 reduction by RBCs requires a consumption of reducing equivalents from intracellular metabolism. The reduction of WST-1 caused a decrease in the metabolic output as gauged by the resultant lactate-to-pyruvate ratio (Figure 6.17). The decrease in this ratio observed for cells incubated with WST-1 in both the presence and absence of PMS is ascribed to an increase in pyruvate production, with little change in the rate of lactate production noted. Hence, it is suggested that the reduction of WST-1 diverts NADH reducing equivalents from the glycolytic pathway. This conclusion is supported by the inhibitory effect of iodoacetate (Figure 6.15). Iodoacetate, by binding cysteines sulfhydryls, inactivates GAPDH which is responsible for the regeneration of NADH from NAD^+ by the reduction of glyceraldehyde 3-phosphate. Inactivation of this enzyme essentially halts glycolysis and inhibits any processes dependent on glycolysis, such as WST-1 reduction.

The recycling of NADPH may also be an important factor for WST-1 reduction in the presence of PMS. The ratio of reduced-to-oxidised glutathione was observed to decrease more rapidly in the presence of WST-1 and PMS than with WST-1 alone or in control cells (Figure 6.16). The increase in GSSG in the RBC suggests that NADPH might be a limiting factor and might be involved in the oxidation of PMS and, consequently, the reduction of WST-1. Alternatively, flux through the oPPP might be reduced due to glycolysis imposing an increased requirement for NADH.

In RBCs the reduction of WST-1 can not be observed directly by ^{1}H NMR spectroscopy. Although WST-1 in aqueous solution has distinct ^{1}H NMR resonances in the aromatic region of the spectrum (Figure 6.3), upon its addition to RBC suspensions these resonances were not observable in ^{1}H Hahn spin-echo spectra with a spin echo delay (τ) of 60 ms (Figure 6.8). Using a spin-echo delay of 60 ms yields minimal signal from large molecules and resonances from freely tumbling endogenous metabolites predominate. However, should a small molecule bind a large molecule it is unlikely to yield equivalent resonances, unless the free and bound species are in fast exchange on the NMR timescale. A spin-echo delay of 20 ms allowed more signal from large molecules to be observed (and favourably altered the *J*-modulation effects). Hence, resonances from a bound small molecule are more likely to be observed, however, resonances from WST-1 were not evident in such spectra either (Figure 6.9). The application of a CPMG pulse sequence (Figure 6.10), a variation of the Hahn spin-echo containing a train of 180° pulses prior to signal acquisition, removes effects due to *J*-coupling, and with a 20 ms delay time for RBC suspensions, allows some signals from large molecules to be observed. The lack of observable WST-1 peaks in RBC suspensions using these three different acquisition conditions suggested that WST-1 was bound to the plasma membrane or proteins in the plasma membrane. This idea was tested by acquiring CPMG spectra of WST-1 in the presence of BSA (Figure 6.11). The absence of distinct WST-1 peaks, and the presence of peaks from the (proposed) contaminant 1,4-oxathiane, in a solution containing BSA, confirmed that WST-1 was indeed able to bind this protein. Thus, despite its anticipated suitability, ^{1}H NMR was shown not to be suitable for the study of WST-1 reduction in RBC suspensions.

The rate of RBC-mediated WST-1 reduction varied in blood samples taken from different mammalian species (Figure 6.18). Human RBCs had the highest WST-1 reduction rate (± PMS), followed by sheep, cattle and horse RBCs, while kangaroo RBCs had very low rates of WST-1 reduction. Within each species there was also variation between the rate of WST-1 reduction between individuals, which for the humans tested (n = 6), did not correlate with age or sex. The rate of WST-1 reduction by the different animal species also did not correlate with the rates of metHb reduction reported in Chapter 5. Compared with human RBCs, metHb

reduction rates in the presence of NADH were low for cattle and horse RBCs, while their WST-1 reduction rates were of a similar magnitude. This suggests that the rate of WST-1 reduction does not depend on the LDH activity, which was a factor for MetHb reduction in the RBCs of different animals (§5.3.6). The different rates of WST-1 reduction activity for the animal species are therefore most likely to be a combination of (1) the glycolytic rate of the RBCs of the animals tested, (2) the activity of the transmembrane WST-1 reductase (NADH oxidase) system, (3) the age and handling of the blood cell sample.

The reduction of WST-1 observed in RBC membranes does not appear to be caused by the NADH oxidase activities reported by Berridge and Tan (1998). The RBC WST-1 reduction rate shows a differing sensitivity to capsaicin than was displayed by the transmembrane NADH-oxidase of transformed and non-transformed cell lines. The changes in the intracellular metabolic state do, however, suggest the involvement of intracellular NADH, which may be transferring reducing equivalents across the plasma membrane to WST-1, as is observed for transmembrane NADH oxidase activity (Berridge and Tan, 1998). An enzyme which reduces WST-1 has been identified and purified from a preparation of rat epididymal sperm; it is cytochrome *P*-450 reductase (Baker, *et al.*, 2004a). The isolated enzyme reduces WST-1 in the presence of NADPH and is inhibited by pCMBS and diphenylene iodonium (a flavoprotein inhibitor), and also by SOD despite the fact that cytochrome *P*-450 reductase does not produce ROS (Baker, *et al.*, 2004a). This WST-1 cytochrome *P*-450 reductase activity may be, or be related to, the cell surface NADH oxidase activity described by Berridge and Tan (2000b). The transmembrane NADH oxidase activity appears to be distinct given that this activity can be inhibited by capsaicin (Berridge and Tan, 1998, 2000b). PMS can also be replaced by Coenzyme Q_1 (a short chain homologue of CoQ_{10}) for the cellular reduction of WST-1 (Tan and Berridge, 2004), hence, it is possible that WST-1 reduction involves quinones and the activity of an NADH:quinone reductase (Tan and Berridge, 2004). The lack of inhibition of the reduction of WST-1 by RBC plasma membranes observed in this study by either capsaicin or pCMBS, suggests a mechanism that is yet to be identified for RBC WST-1 reduction, which may differ from those previously reported.